

Fractional-order integral resonant control of collocated smart structures

D. Feliu-Talegon^b, A. San-Millan^b, V. Feliu-Battle,^{a,*}

^a*Escuela Técnica Superior de Ingenieros Industriales, Universidad de Castilla-La Mancha, Ciudad Real, 13071 Spain*

^b*Instituto de Investigaciones Energéticas y Aplicaciones Industriales (INEI), Campus Universitario de Ciudad Real, 13071 Ciudad Real, Spain*

Abstract

This paper proposes a fractional-order integral controller, FI, which is a simple, robust and well-performing technique for vibration control in smart structures with collocated sensors and actuators. This new methodology is compared with the most relevant controllers for smart structures. We demonstrate that the proposed controller improves the robustness of the closed-loop system to changes in the mass of the payload at the tip. The previous controllers are robust in the sense of being insensitive to spillover and maintaining the closed-loop stability when changes occur in the plant parameters. However, the phase margin of such closed-loop systems (and, therefore, their damping) may change significantly as a result of these parameter variations. In this paper we explore the possibility of increasing the phase margin robustness by using a fractional-order controller with a very simple structure. We have applied this controller to an experimental smart structure, and simulations and experiments have shown the improvement attained with this new technique in the removal of the vibration in the structure when the mass of the payload at the tip changes.

Keywords: fractional-order control; smart structures; active vibration damping; piezoelectric actuators; strain gauges; robust control.

1. Introduction

There are many industrial and scientific applications for which very lightweight mechanical structures are needed. These are built from lightweight materials with a small cross section. However, the performance of these structures may be impaired because they are prone to undamped vibrations and noises; see for example Moheimani & Fleming (2005), Vepa (2010). Smart structures, or structures with integrated sensors and actuators, are a technical solution which efficiently damps mechanical vibrations in applications in which passive techniques are either insufficient or impractical. Examples of these smart structures are nanopositioning devices in scanning probe microscopes Fleming et al. (2010), large telescopes Preumont et al. (2009), active noise cancellation systems in vibroacoustics Tokhi & Veres (2002) or precision machines Quintana & Ciurana (2011).

The most common class of smart structures are those with integrated piezoelectric actuators and sensors. Their small volume, low weight and ease of structural integration, signify that piezoelectric sensors and

actuators are very often used as transducers in smart structures. It is well known that there are a number of difficulties associated with the control of flexible structures, the foremost being: variable resonance frequencies; high system order - which implies the risk of destabilizing systems with high-frequency dynamics (spillover effect), and highly resonant dynamics Aphale et al. (2007). Traditional control system design techniques such as LQG, H_2 and H_∞ have been applied to control these structures; see for example Banks et al. (1996), Petersen & Pota (2003), Halim & Moheimani (2002b), Ghosh et al. (2015), Halim & Moheimani (2002a), Zhu et al. (2009). Unfortunately, the direct application of such techniques has the tendency to produce control systems of a high order and possibly poor stability margins. Other techniques address Lyapunov based techniques Preumont (2011) so as to guarantee stability, or flatness based control Meurer et al. (2008) for trajectory tracking that is robust to spillover effects.

A different approach is that of attempting to take advantage of the properties of collocated resonant mechanical systems in order to design robust control systems. The most useful characteristic of a collocated system is the interlacing of poles and zeros up the $j\omega$ axis (IPZ property). This results in a phase response that

*Corresponding author

Email address: Vicente.Feliu@uclm.es ()

lies continuously between 0° and 180° . Some control techniques have been developed that exploit this property, yielding controllers with significantly more robust properties while having simpler structures than those mentioned previously. In particular, some of these controllers make it possible to address the spillover problem in a quite straightforward manner. We have therefore focused our research on this class of controllers. The most relevant controllers for smart structures that use the IPZ property are presented as follows.

Positive position feedback (PPF) is one of the control techniques to use the IPZ property and to have found a practical application. This technique was first introduced in Goh & Caughey (1985). PPF is essentially a second-order filter, which has proven to be an effective vibration control method for flexible systems embedded with smart materials Fanson & Caughey (1990), Chu & Cui (2015). PPF controllers are stable in the presence of uncontrolled in-bandwidth modes, and roll off quickly at higher frequencies, thus reducing the risk of spillover. A modification of this controller, denoted as the MPPF controller, was proposed in Nima Mahmoodi & Ahmadian (2009) in order to improve the active damping. An adaptive version of the MPPF was later proposed in Nima Mahmoodi et al. (2010). Another control technique is Velocity feedback (VF). Bar-Kana et al. (1991) proved that this technique could remove vibrations even in the case of totally undamped structures and Omidi et al. (2015) is a recent example of a practical application. VF attempts to introduce damping in the system. However, one drawback of the controller involved is that its high-frequency gain must be attenuated so as to avoid noise amplification and destabilization owing to unmodeled or non-collocated dynamics. Two additional poles must therefore be added to the controller, which often yield a relatively low performance and a poor phase margin. Another approach is the resonant control (RC), which guarantees closed-loop stability in the presence of uncontrolled out-of-band modes of the structure. This has been successfully applied to collocated resonant systems Pota et al. (2002), but the high-pass nature of the controller may impede its use in certain applications. An improvement to this technique is the integral resonant control (IRC). This controller significantly augments the damping provided by the RC while maintaining the rolling off feature at higher frequencies.

The previous controllers are robust in the sense of being insensitive to spillover and maintaining the closed-loop stability when changes occur in the plant parameters. However, the phase margin of these closed-loop systems (and, therefore, their damping) may change sig-

nificantly with these parameter variations. In this paper, we explore the possibility of increasing the phase margin robustness by using a fractional-order controller with a very simple structure.

The previous work carried out on the control of flexible structures and robots showed the increase in robustness that can be achieved by using fractional-order controllers. For example, a fractional-order proportional-derivative controller was proposed by Manabe Manabe (2002) for a flexible spacecraft attitude control; controllers that include a proportional term plus two fractional-order derivative terms of different orders were designed by Valerio (2005) to control a planar two degrees of freedom flexible robot; a fractional-order proportional-derivative controller was also used by Monje et al. (2007) for the control robust of payload changes of a single link flexible robot, while an analog device denoted as a "fractor" was proposed by Bohanan (2008) to control a flexible link using a fractional-order proportional-integral controller. Despite the fact that fractional-order controllers can improve the robustness of control systems, none of the previous controllers guarantee robustness to spillover effects. We should also mention several methods with which to tune fractional-order controllers with simple structures that already exist. Fractional-order *PI* controllers that achieve nominal phase margin and gain crossover frequency specifications or nominal gain margin and phase crossover frequency specifications, together with local robustness to plant gain changes were proposed by Monje et al. (2004). Phase-lead and phase-lag compensators that achieved nominal phase margin and gain crossover frequency specifications, together with local robustness to plant gain changes and low and high frequency disturbance rejection were also developed by Monje et al. (2008). Padula & Visioli (2012) proposed tuning rules so as to optimize certain integral control performance indexes applied to integral and unstable processes. More recently, Tavazoei & Tavakoli-Kakhki (2014) developed some conditions for the simultaneous achievement of desired phase and gain margins with fractional-order compensators. We should state that all these methods - and others that also exist in scientific literature - are not as well suited to controlling systems as that studied in this work, which consists of an infinite dimensional system with very lowly damped vibration modes.

This paper therefore presents the development of a new control scheme for collocated smart structures, which achieves higher robustness by using a fractional-order controller. The robustness is achieved in the phase margin and, equivalently, in the damping of the closed-

loop system. In order to assess the advantages attained by this controller, its performance is compared with the performances achieved by three techniques that simultaneously share the following features: 1) they propose controllers that are robust to spillover effects, 2) they have robust stability to large parametric variations, 3) the controllers yielded are linear and the methodology used in their design is relatively simple, and 4) they are highly recognized works in the smart material structures scientific community, and are considered as reference methods with which to control beam structures with piezoelectrics. These three techniques are the aforementioned IRC, PPF and MPPF control schemes.

This paper is organized as follows. Section 2 describes the experimental setup. Section 3 develops the dynamic modeling and identification of the platform. Section 4 presents the three well-known techniques with which to control collocated smart structures, Section 5 develops our new fractional-order controller. Section 6 presents simulated and experimental results using the three proposed controllers and Section 7 outlines some conclusions.

2. Experimental system

The experimental smart structure consists of a flexible aluminium cantilevered beam which is clamped at one end (the base of the beam) and is free at the other end (the tip of the beam). We should mention that the clamped end is attached to a DC motor that is not used in the experiments shown in this paper. This DC motor is braked. We therefore assume that the clamped end of the beam is quiet. This structure is shown in Figure 1 and is composed of:

- The uniform flexible beam.
- Strain gauges placed at the base of the beam to measure the torque at that point of the structure.
- Piezoelectric actuators placed at the base of the beam (hereafter denoted as PEA), whose purpose is to apply torque to the structure in order to remove existing mechanical vibrations.
- A Polytec LDV (model OFV-5000) with a sensor head of model "OFV-534 Compact Sensor Head" which measures the displacement and velocity of the free end of the beam (laser vibrometer).

The whole system is regarded as a Single-input Single-output system (SISO). The input (control signal) is the voltage applied to the piezoelectric actuators and

the output (controlled signal) is the voltage measured by the gauges located at the base of the beam. Moreover, since we are concerned with the precision and vibration cancellation achieved at the tip of the structure, the Polytec sensor provides measurements of this point. These last measurements are not fed back for control purposes, and are used solely to verify the performance of the controlled system. The features of the beam are shown in Table 1.

Table 1: Parameters of the flexible arm

Stiffness ($N \cdot m^2$)	EI	2.40
Width (m)	h	0.05
thickness (m)	b	0.002
Length (m)	L	1.26
Linear density (kg/m)	ρ	0.268
Mass of the beam (Kg)	M_b	0.338
Payload mass (Kg)	M_p	[0.0, 0.3]
Payload rotational inertia ($Kg \cdot m^2$)	J_p	[0.0, $4.7 \cdot 10^{-5}$]

The data obtained from the experimental platform was computed in real time using a PC equipped with LabView and an acquisition card of the PCI-6221 type.

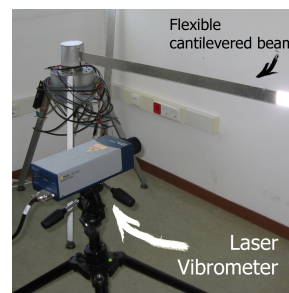


Figure 1: Picture of the experimental platform.

3. Modelling and identification of the platform

3.1. Dynamic model

The linearized equations of motion can be derived from energy equations and the Hamilton principle (note that the movement is constrained to the horizontal plane and the gravity effects are negligible). For the system represented in Figure 2, these equations are:

$$\frac{\partial^2}{\partial x^2} \left(EI \frac{\partial^2 w(x,t)}{\partial x^2} \right) + \rho \frac{\partial^2 w(x,t)}{\partial t^2} = q_y(x,t) \quad (1)$$

$$q_y(x,t) = -\frac{\partial}{\partial x} \left(\frac{\partial \tau_p}{\partial x} \right) \quad (2)$$

where ρ is the link density per unit length, $w(x,t)$ is the elastic displacement (at a point x in a time t), EI is the link flexural rigidity, and τ_p is the torque induced by the piezoelectric actuator and may be assumed to be a constant throughout the extent of the patch comprised between the coordinates x_1 and x_2 . This moment is modeled as:

$$\tau_p = -\mu\rho(H(x-x_1) - H(x-x_2))V_p(t) \quad (3)$$

where $H(x-x_i)$ is the Heaviside step function starting at the coordinate x_i , μ is the moment of the patch per unit linear density of the beam and per unit of applied voltage for the actuator patch, and $V_p(t)$ is the voltage applied to the piezoelectric actuator.

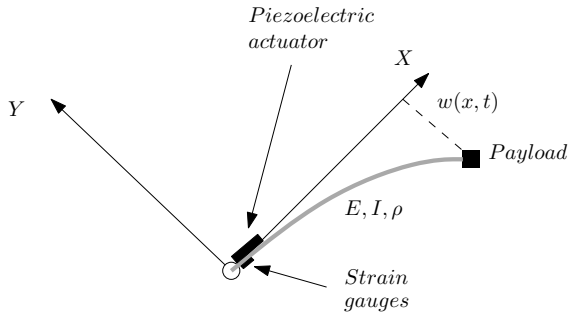


Figure 2: Scheme of the flexible beam.

The geometrical and natural border conditions are:

$$w(t,0) = 0 \quad (4)$$

$$\frac{\partial w}{\partial x}(t,0) = 0 \quad (5)$$

$$EI \frac{\partial^2 w}{\partial x^2}(t,L) = -J_p \frac{\partial}{\partial x} \left(\frac{\partial^2 w(t,L)}{\partial t^2} \right) \quad (6)$$

$$EI \frac{\partial^3 w}{\partial x^3}(t,L) = M_p \frac{\partial^2 w(t,L)}{\partial t^2} \quad (7)$$

where the parameters of these equations are the payload mass M_p , link length L , and rotational inertia of the payload J_p

The dynamical model of the whole system can be obtained by solving the above boundary value problem. This was done in Pota & Alberts (1995), in which the exact transfer functions for a flexible slewing link piezoelectric laminate were presented. The resulting transcendental forms of transfer functions represented six

input/output pair combinations for a slewing flexible beam with a DC motor and a piezoelectric actuator as inputs, and the motor angle, the bending moment at the location of the piezoelectric actuator and the tip position as outputs (sensed variables). In the special case in which the hinged end is clamped, these results yield the desired transfer function between the piezoelectric actuator and the strain gauge measurement of the bending moment at the base of our one-end-clamped link. In Pota & Alberts (1995), the resulting transfers functions were reduced to a rational form using Maclaurin series expansions. This process yields an infinite number of vibration modes.

In our system, since the piezoelectric actuator and the strain gauge sensor are placed in the same position, they constitute a collocated actuator-sensor pair. It is possible to show (e.g. Aphale et al. (2007), Preumont (2011)) that, in this special case, the rational transfer function which relates the input to the system (i.e., the voltage applied to the PEA) and the output of the system (i.e., the strain measured at the base of the beam, $V_g(t)$, given in volts) resulting from the above Maclaurin series expansion has the form

$$\frac{V_g(s)}{V_p(s)} = G(s) = \sum_{i=1}^N \frac{\alpha_i}{s^2 + 2\xi_i \omega_i s + \omega_i^2} + D, \quad (8)$$

where D is a real number, $N = \infty$, and it is verified that parameters α_i , ω_i and ξ_i - which are respectively the gains, the natural frequencies and the damping coefficients associated with each vibration mode of the beam - are equal to or greater than zero. This infinite dimensional transfer function is often approximated by means of a modal discretization, in which expression (8) still holds but N is now a finite number. Note that this transfer function has $2N$ poles and $2N$ zeros.

Another property of collocated systems is the interlacing of poles and zeros up the $j\omega$ axis, e.g. Aphale et al. (2007). Let us denote the N pairs of complex conjugate poles of (8) as p_i and p_i^* , $1 \leq i \leq N$, and the N pairs of complex conjugate zeros of this model as z_i and z_i^* , $1 \leq i \leq N$. This interlacing property therefore signifies that $\Im(p_i) < \Im(z_i) < \Im(p_{i+1})$ for $1 \leq i < N$ and $\Im(p_N) < \Im(z_N)$. This results in a phase response that lies continuously between 0° and 180° .

We should state that the controller developed in Section 5 and the three controllers proposed for comparison are robust to spillover. They are therefore derived by taking into account the transfer function (8) with $N = \infty$, and the properties of collocated systems are used.

However, the dynamics of our experimental setup is

approximated by a truncated model that includes only four vibration modes corresponding to the four lowest vibration frequencies. This truncated model will be used to tune the parameters of the controllers in order to attain transient specifications (although it should be noted that spillover robustness will be guaranteed in these controllers), and to run simulations in order to show approximate though sufficiently accurate time responses of the closed-loop systems.

3.2. Identification

The values of the parameters of model (8) with $N = 4$ are obtained from an experimental identification process which was performed on the experimental platform for three different cases: a) without a payload, b) with a payload at the tip of 0.15 kg ($J_p = 0.2343 \cdot 10^{-4} \text{ Kg} \cdot \text{m}^2$) and c) with a payload at the tip of 0.3 kg ($J_p = 0.4686 \cdot 10^{-4} \text{ Kg} \cdot \text{m}^2$). Three transfer functions, $G_i(s)$, $1 \leq i \leq 3$, were therefore estimated using the data recorded in the experiments in which the beam was moved with any of these three payloads attached to its tip. Of the different methods with which to carry out this identification process that can be found in scientific literature, the method described in Piersol & Bendat (1993) has been employed in this paper because it is easy to use and is well suited to systems with little damping and very decoupled vibration modes. This identification process was performed using a Chirp signal as input (V_p), which stimulated the different vibration modes. This signal has an amplitude of 0.02 volts and a range of frequencies from 0.1 Hz to 50 Hz in 100 s. Model (8) was then fitted to the frequency responses experimentally obtained for all the payloads. This process yielded the values of the parameters of the model shown in Table 2 for the three payloads. In this process, parameter D was assumed to be the same in the three transfer functions $G_i(s)$. The value identified was $D = 0.038$.

The magnitude of the frequency response between V_p and V_g obtained in experimentation in the case of the beam without a payload at the tip and the magnitude of the frequency response of the approximated model are shown in the upper half of Figure 3. The experimental phase of this frequency response and that of the approximated model are shown in the lower half of Figure 3.

These figures show that the frequency response of the fitted model with four vibration modes describes the experimental frequency response very well, and equation (8) therefore accurately captures the dynamics of our mechanical structure. A small difference between the model and the experimental phases, that linearly increases with frequency, can be observed in the lower

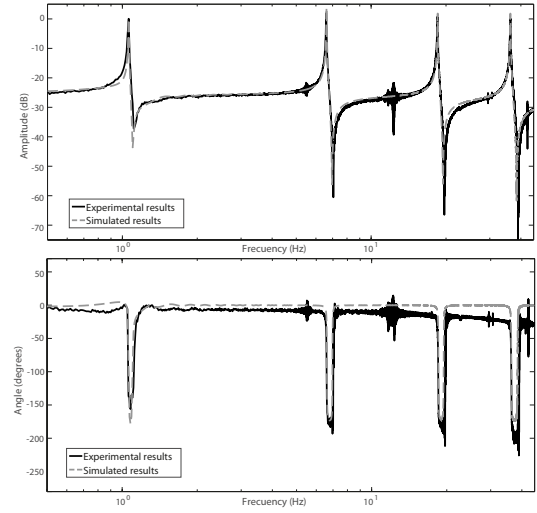


Figure 3: Identification of the platform.

half of Figure 3. This is caused by a delay of 2 ms that is present in the dynamics of the system. The effect of this delay is negligible in the range of frequencies considered in this study and is not therefore taken into account. Similar results were obtained in the cases of the beam with payloads of 0.15 kg and 0.3 kg.

The Nyquist plot of transfer function (8) with the parameters shown in Table 2 yields drawings like that shown in Figure 4, whose phase changes between 0° and -180° for values $0 \leq \omega < \infty$. The phase margins achieved are: 41.8° for a payload of 0 kg, 39.5° for a payload of 0.15 kg and 35.3° for a payload of 0.3 kg.

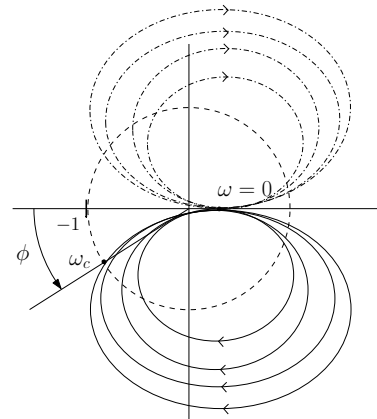


Figure 4: Nyquist of $G(s)$.

i	$M_p = 0.0kg$ ($G_1(s)$)			$M_p = 0.15kg$ ($G_2(s)$)			$M_p = 0.3kg$ ($G_3(s)$)		
	α_i	ξ_i	ω_i	α_i	ξ_i	ω_i	α_i	ξ_i	ω_i
1	0.24	0.002	6.66	0.068	0.0017	3.96	0.036	0.0012	2.89
2	8.8	0.0016	41.58	5.5	0.0015	32.87	4.5	0.0013	30.74
3	60	0.0018	116.36	55	0.0043	101.16	40	0.002	98.71
4	232	0.0018	228.1	160	0.0018	206.1	150	0.0018	202.9

Table 2: Identification

4. Three well-known controllers

This section introduces three control schemes with which to cancel mechanical vibrations in smart structures: the IRC, PPF and MPPF controllers. Of all the methods that can be found in scientific literature, these three have been chosen because they have the following properties: 1) they yield simple controllers, 2) they efficiently remove the vibrations in mechanical structures which have collocated sensors and actuators, 3) they are robust to spillover and 4) their stability is robust to large variations in the plant parameters. Properties 3) and 4) are the main issues in this paper, and these methods are the best suited to achieving them.

The main objective of the previous control techniques is to damp the low-frequency vibration modes of mechanical systems that exhibit the IPZ property. In this section, a controller is designed for each of these control schemes. The performances of these controllers will later be compared with the performance of the fractional-order controller proposed in this paper.

Since no very definite criteria with which to tune the controllers gains are provided in these methods, a clear design criterion, common to all the controllers studied here, is proposed in this paper. This will allow us to carry out a fair comparison of the controllers' performances.

Since we have identified four vibration modes in the system transfer function (an eighth order model), and the first vibration mode is that which yields the vibrations of greatest amplitude, the proposed design criterion is to damp the first (lowest) vibration mode as much as possible. Note that, since we are considering control schemes that are robust to spillover, second, third and fourth vibration modes will not unstabilize the closed-loop control system. Moreover, these control systems introduce some damping in modes that are higher than the first one (although they cannot guarantee a minimum damping in these high order modes).

Second, third and fourth vibration modes (and even higher modes that have not been detected) will not

therefore be taken into account in the design of the controllers (only in the IRC in order to attain the spillover rejection property). These modes will be taken into account only to assess that there are no spillover effects. All the following controllers are designed for a payload of 0 kg at the end of the beam, which is considered to be the nominal plant.

4.1. Integral resonant control (IRC)

The main objective of this control system is to damp the low-frequency modes of a collocated resonant mechanical system with interlaced poles and zeros in the imaginary axis. The schematic diagram of this control technique is shown in Figure 5, where P is a disturbance in the system.

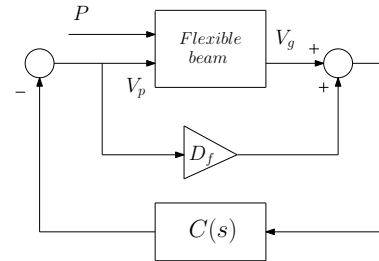


Figure 5: Schematic diagram of IRC.

The design of the controller $C(s)$ and the gain D_f in Figure 5 is explained in Aphale et al. (2007). We have applied the IRC design procedure in the following steps:

1. Determine the required feed-through term D_f that adds a pair of complex nearly imaginary zeros at a frequency lower than the first resonant mode of the system. This step produces the phase inversion of the original transfer function in such a way that the phase of the modified transfer function again lies between 0° and -180° , but changes in the opposite direction. In order to achieve this simultaneously for the three tip payloads (robust design), D_f is calculated such that the previous effect is obtained in

the three $G_i(s)$, $1 \leq i \leq 3$). The maximum damping is achieved with a value of $D_f = -0.0574$, which is on the border of the range of admissible values. A value of $D_f = -0.0588$ is therefore chosen, which maintains a security margin of 2.5% of the previous value in order to guarantee the closed-loop stability of the system in the case of small inaccuracies in the model identified.

- Design the controller of the form $C(s) = \frac{-\gamma s}{(s+q)^2}$, tuning q to be approximately a decade lower than the frequency of the first vibration mode ($q \simeq \omega_1/10$) and selecting a suitable gain γ which damps the first mode as much as possible. The controller designed is:

$$C(s) = \frac{-873.4s}{(s+2.151)^2}. \quad (9)$$

4.2. Positive position feedback (PPF)

The main objective of this control system is to damp the low-frequency modes of a collocated resonant mechanical system with the IPZ property. The schematic diagram of this technique is shown in Figure 6. The use of a PPF controller has the following advantages: a) it provides quick damping for a particular mode if the natural frequencies of the system are well known, b) it is insensitive to spillover, c) PPF is easy to implement. These advantages signify that PPF controllers have been widely applied to flexible systems with collocated actuator-sensor pairs in order to achieve active damping.

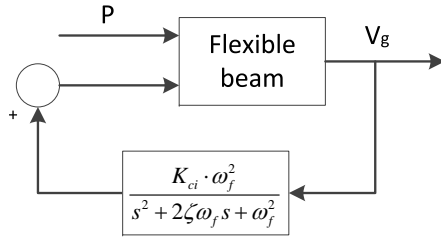


Figure 6: Schematic diagram of PPF.

Several procedures with which to tune the parameters of this controller have been proposed. For example, Friswell & Inman (1999) stated that a PPF controller can be formulated as an output feedback controller and control design algorithms for output feedback systems can therefore be used to design PPF controllers; and McEver & Leo (2001) proposed an autonomous tuning by using an optimal feedback compensator combined with an on-line pole-zero identification.

The parameters of the PPF controller used in our smart structure were tuned in such a way that the damping of the first vibration mode was maximized. The same design approach of the IRC was therefore used in this controller. This criterion was achieved by placing the closed-loop poles corresponding to the first vibration mode as far as possible from the imaginary axis.

The controller designed using the aforementioned procedure has the following parameters:

$$PPF(s) = \frac{54774.72}{s^2 + 33.1s + 3247.64} \quad (10)$$

4.3. Modified Positive position feedback (MPPF)

This control technique is based on the conventional PPF and was first proposed in Nima Mahmoodi & Ahmadian (2009). The MPPF controller is a combination of the second order compensator used in the PPF and a first order compensator that increases the damping of the system. The two compensators are connected in parallel, as shown in Figure 7, and their gains, g and h , are tuned to adjust the stiffness and damping of the closed loop system. Moreover, the first order compensator was added with the aim of lowering the steady-state error produced by the application of persistent disturbances $P(t)$ Nima Mahmoodi et al. (2010).

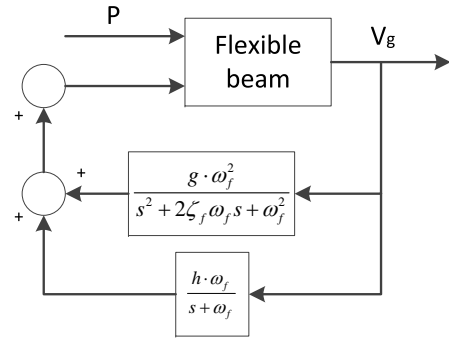


Figure 7: Schematic diagram of MPPF.

In order to tune this controller, the frequency and the damping of the filters took the same value as in the case of the PPF controller, and the gains of the two filters were chosen by means of an optimization procedure so that the the damping of the first vibration mode was maximized. It will be noted that the same design approach as that of the IRC and PPF controllers has been utilized.

The controller designed using the aforementioned procedure has the following parameters:

$$MPPF_1(s) = \frac{43820}{s^2 + 33.1s + 3247.64} \quad (11)$$

$$MPPF_2(s) = \frac{171}{s + 56.99} \quad (12)$$

5. New fractional-order controller

The frequency specifications obtained with the previous controllers are shown in Table 3 for the different payloads. In particular, this table shows that: 1) the phase margin greatly changes according to the payload in the IRC, becoming smaller (its absolute value) as the payload mass increases - in fact, it becomes very small for a payload of 0.3 kg - and 2) the phase margins of the PPF and the MPPF are always very small. In this section, our objective is therefore to create a new methodology in order to improve the robustness of the closed-loop system to changes in the mass of the payload at the tip.

5.1. Motivation for using a fractional-order integral controller

The basic idea of our methodology is to approximately rotate the Nyquist plot shown in Figure 4 in the direction required in order to increase the phase margin, which implies increasing the damping and, indirectly, reducing the settling time. We are also interested in a controller having a proper transfer function that, moreover, does not have a pure derivative action in its numerator. This is necessary because the measurements of strain gauges are noisy (a small level of noise remains even after proper filtering and amplification) and, if they are feedback, the noise may be amplified, producing excessive control signals that could saturate the piezoelectric actuator, and thus deteriorating the control performance.

Approximate rotations of the part of the Nyquist plot which is the mapping of the path traveling up the $j\omega$ axis from 0 to $j\infty$ can be achieved by using controllers of the form

$$C_{CPE}(s) = K_\alpha s^\alpha \quad (13)$$

This transfer function has a frequency response with a constant phase in all the range of $0 \leq \omega < \infty$, and it is known as the constant phase element (hereafter denoted as *CPE*, Cole (1933)). We should mention that other transfer functions besides (13) can be used to implement *CPEs*, see e.g., Feliu & Feliu (1997). The proper transfer function condition is achieved by making $\alpha < 0$ in (13).

In order to improve the phase margin of the Nyquist plot shown in Figure 4, it would be necessary to produce a counterclockwise rotation. This would imply using a controller (13) with $\alpha > 0$, i.e., a fractional-order derivative action, which is not permitted owing to the reasons stated previously.

We therefore propose modifying the open-loop transfer function in the same way as occurs in the IRC technique (see Figure 5), i.e., first add a negative constant D_f to the open-loop transfer function, and second multiply the result by -1 .

Once the transfer function has been modified, a *CPE* controller is designed. The rationale behind this procedure is the following. Let us define the modified transfer function $G_u(s) = -(G(s) + D_f)$. Its Nyquist diagram is shown in Figure 8. In this diagram, the phase changes between 0° and $+180^\circ$ for the values $0 \leq \omega < \infty$. If a controller $C'(s)$ that has a constant phase θ in all $0 \leq \omega < \infty$ were used, the phase of the Nyquist plot of $G_u(s) \cdot C'(s)$ would change between θ° and $\theta^\circ + 180^\circ$ for values $0 \leq \omega < \infty$.

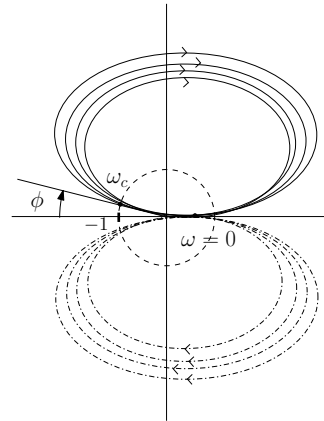


Figure 8: Nyquist diagram of $G_u(s)$.

Moreover, Figure 8 suggests that, if θ were a negative value, the part of the Nyquist diagram that lies in the left half-plane would move away from the point $(-1, 0)$. What is more, the part of the diagram that lies in the right half-plane would cross the positive real abscissa, but this is irrelevant for relative stability purposes.

This negative constant phase controller (negative *CPE* controller) can be implemented by means of the transfer function:

$$C'(s) = \frac{K_\alpha}{s^\alpha} \quad (14)$$

where $K_\alpha > 0$ and the fractional order α is comprised in the interval $\in [0, 2]$ in order to achieve the stability of the

	IRC (0kg)	IRC (0.15kg)	IRC (0.3kg)	PPF (0kg)	PPF (0.15kg)	PPF (0.3kg)	MPPF (0kg)	MPPF (0.15kg)	MPPF (0.3kg)	FI (0kg)	FI (0.15kg)	FI (0.3kg)
$\phi_M(^{\circ})$	-45.8	-22.26	-6.8	-2	-1.5	-1.2	-2.67	-1.84	-1.48	-113.4	-113.6	-113.9
$\omega_c(\text{rad/s})$	5.18	3.15	2.37	3.25	2.42	2.05	3.98	2.73	2.18	4.94	2.88	2.194
M_g	∞	∞	∞	1.03	1.05	1.08	1.06	1.07	1.11	∞	∞	∞
$\omega_g(\text{rad/s})$	—	—	—	0	0	0	0	0	0	—	—	—

Table 3: Simulation data

closed-loop system. This is denoted as the fractional-order integral controller (*FI* controller), and it produces a clockwise rotation of $-\theta = 90\alpha^{\circ}$ in the Nyquist diagram of $G_u(s)$ (of course, it also produces changes in the magnitudes of the diagram). Figure 9, which represents the Nyquist plot of $L(s) = G_u(s) \cdot C'(s)$ if controller (14) were used, shows this effect. Moreover, this fractional-order integral action located in the feedback branch filters the high frequency noises produced by the strain sensor. Note that our control scheme coincides in practice with the scheme of the *IRC* shown in Figure 5, but is implemented with a $C(s) = -C'(s)$.

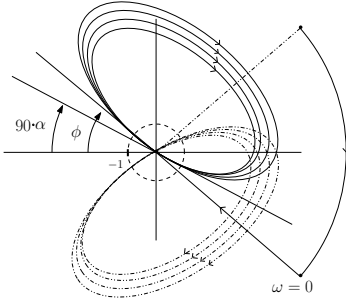


Figure 9: Nyquist diagram of $L(s)$.

Controller (14) therefore subtracts a constant phase equal to $90\alpha^{\circ}$ from the Nyquist diagram in the entire frequency range of $0 \leq \omega \leq \infty$, thus increasing the phase margin of the system (its absolute value).

5.2. The principal result

The properties of the aforementioned proposed controller are demonstrated in the following theorem.

Theorem. Consider a collocated system that has an infinite dimensional transfer function (8) where $N = \infty$. Assume that the parameters $(D, \alpha_i, \xi_i, \omega_i, 1 \leq i < \infty)$ of this transfer function $G(s)$ may undergo large variations (but always $\alpha_i, \xi_i, \omega_i \geq 0$). Denote as Ω the set of all possible infinite dimensional transfer functions allowed by the parametric variations of $G(s)$ ($G \in \Omega$). Assume the *IRC* control scheme shown in Figure 5, in which the controller is of the form

$$C(s) = -\frac{K_\alpha}{s^\alpha} \quad (15)$$

where $K_\alpha > 0$ and $0 < \alpha \leq 1$, and the feed-through term verifies the condition

$$D_f < -\max_{G \in \Omega} G(0) \quad (16)$$

This control system verifies that for any $G \in \Omega$: 1) the closed-loop system is stable, 2) its phase margin is $\phi_M \leq -90 \cdot \alpha$ and 3) the gain margin is ∞ .

Proof. The characteristic equation of this control system is

$$1 + \underbrace{\frac{-K_\alpha}{s^\alpha} \left(\sum_{i=1}^{\infty} \frac{\alpha_i}{s^2 + 2\xi_i \omega_i s + \omega_i^2} + D + D_f \right)}_{L(s)} = 0 \quad (17)$$

Moreover, we have that

$$G(0) = \sum_{i=1}^{\infty} \frac{\alpha_i}{\omega_i^2} + D \quad (18)$$

The beam transfer function can therefore be expressed as

$$G(s) = G(0) - s \sum_{i=1}^{\infty} \frac{\alpha_i}{\omega_i^2} \frac{s + 2\xi_i \omega_i}{s^2 + 2\xi_i \omega_i s + \omega_i^2} \quad (19)$$

and the open-loop frequency response $L(\omega)$ is

$$L(\omega) = \frac{K_\alpha}{(j\omega)^\alpha} (-G(0) - D_f + \Psi(\omega)) \quad (20)$$

where

$$\Psi(\omega) = \sum_{i=1}^{\infty} \frac{\alpha_i}{\omega_i^2} \frac{-\omega^2 + j2\xi_i \omega_i \omega}{(j\omega)^2 + 2\xi_i \omega_i (j\omega) + \omega_i^2} \quad (21)$$

Upon operating this expression, we obtain that

$$\Im(\Psi(\omega)) = \sum_{i=1}^{\infty} \frac{2\alpha_i \xi_i \omega_i \omega}{(\omega_i^2 - \omega^2)^2 + (2\xi_i \omega_i \omega)^2} > 0 \quad (22)$$

which is clearly verified for values $0 \leq \omega < \infty$. This implies that the phase of $\Psi(\omega)$ is comprised between 0° and 180° for this frequency range, and this is therefore also so for the phase of $-G(0) - D_f + \Psi(\omega)$. Since $(j\omega)^\alpha = \omega^\alpha e^{j\frac{\pi}{2}\alpha}$, we obtain that

$$-90\alpha^\circ \leq \angle L(\omega) \leq 90(2 - \alpha)^\circ, \quad 0 < \omega < \infty, \quad (23)$$

which is verified for any $G \in \Omega$.

Bearing in mind that $\lim_{\omega \rightarrow 0} K_\alpha \Psi(\omega)/(j\omega)^\alpha < \infty$ because $\alpha \leq 1$, the mapping through $L(s)$ of the Nyquist detour around the origin is given by $K_\alpha(-G(0) - D_f)/(j\omega)^\alpha$. If D_f is chosen such that (16) is verified, then $-G(0) - D_f > 0$ for any $G \in \Omega$ and the mapping of the detour $\varepsilon e^{j\theta}$, where $\varepsilon \rightarrow 0$ and θ varying from $-\pi/2$ to $\pi/2$, through $L(s)$ is an arc of circumference whose angle varies from $\alpha\pi/2$ to $-\alpha\pi/2$. The mapping of this detour around the origin therefore always remains in the right half of the complex plane and the encirclement of the point $(-1, 0)$ is therefore prevented. The infinite dimensional closed-loop system is consequently stable and the Assertion 1 of the theorem is proven. Moreover, inequality (23) implies the verification of Assertion 2. Finally, this inequality also proves that the real negative semiaxis is never crossed by the Nyquist plot (please recall that the mapping of the detour of the Nyquist contour around the origin always remains in the right half-plane) and the gain margin is therefore infinite. Assertion 3 is therefore also proven. \square

Remark 1: on the robustness of the phase margin. This theorem signifies that this controller, besides increasing the phase margin of the system (its absolute value) for the nominal payload case (0 kg), also significantly increases the robustness of the closed-loop system. Owing to the aforementioned IPZ property of $G(s)$, the proposed control scheme makes the phase margin of the controlled system $\phi \leq -90\alpha^\circ$ for any possible payload at the tip of the beam (for any $G \in \Omega$), thus always preserving a phase margin of at least $-90\alpha^\circ$. It is easy to check that the lower the damping coefficients of the vibration modes of $G(s)$ are, the closer to $-90\alpha^\circ$ the phase margin will be in all the possible plants, and the lower the variations of the phase margin of the system to changes in the plants will be. The only control system that achieves stability robustness

and moreover phase margin robustness is the fractional-order controller proposed here. Other previous controllers - such as the IRC, PPF and MPPF - only achieve stability robustness.

Remark 2: on the spillover robustness. The theorem has been proven for infinite dimensional transfer functions. The spillover effects are therefore avoided by the proposed controller. Note that the results of the theorem are also valid in the case of a finite number of vibration modes ($N < \infty$).

Remark 3. In the case that $1 < \alpha < 2$, it is possible to demonstrate in a similar way to that which occurred in the theorem that: 1) the closed-loop system is stable and 2) the gain margin is ∞ . However, now the phase margin is not necessarily $\phi_M \leq -90 \cdot \alpha$ since the part of the Nyquist plot corresponding to the mapping of the path traveling up the $j\omega$ axis from 0 to $j\infty$ may invade the third quadrant of the complex plane, thus yielding a positive phase margin. In this case, it is guaranteed that this positive phase margin ϕ'_M is bounded by $\phi'_M \geq 90(2 - \alpha)^\circ$. Robust stability and spillover robustness are consequently guaranteed if $1 < \alpha < 2$, for any $G \in \Omega$, and the positive phase margin ϕ'_M is guaranteed to be greater than $90(2 - \alpha)^\circ$ for any $G \in \Omega$.

5.3. Controller design procedure

The design methodology for this new technique is explained as follows:

1. Obtain the range of values of the feed-through term which produces the phase inversion of the original transfer function and maintains the IPZ property for the m transfer functions, as occurred with the IRC technique. This is given by

$$D_f \leq -\max_{1 \leq i \leq m} G_i(0) \quad (24)$$

The same value of $D_f = -0.0588$ that was obtained in the IRC controller is used here.

2. Choose the values of K_α and α which provide the maximum damping in the first vibration mode of the beam.

The final controller is, therefore:

$$C(s) = -\frac{1392.72}{s^{1.25}} \quad (25)$$

which implies that the phase margin is always lower than $-90\alpha = -112.5^\circ$. Note that $\alpha > 1$ which, according to the Remark 3, may imply that a positive phase margin ϕ'_M may appear that lowers the relative stability of the system. During the controller design process,

we have checked that, for the four vibration modes considered in $G_1(s)$ (the nominal plant), the phase of the Nyquist plot corresponding to the mapping of the path traveling up the $j\omega$ axis from 0 to $j\infty$ is always greater than $-90(2 - \alpha)^\circ$. The phase margin is therefore negative and smaller than -90α in the case of the nominal plant. Figure 10 shows a sketch of the Nyquist plot of the open-loop transfer function $L(s)$ corresponding to the application of the FI controller to the $G_i(s)$ plants (the four vibration modes are considered). The points of the Nyquist plot that cross the unity circumference (which define the phase margin) are labeled as "Pn" in this figure, and the values of the phases at these points are shown in Table 4. This table shows that the Remark 3 is verified: all the phases in all the $G_i(s)$ are bigger than $-90(2 - \alpha)^\circ = -112.5^\circ$.

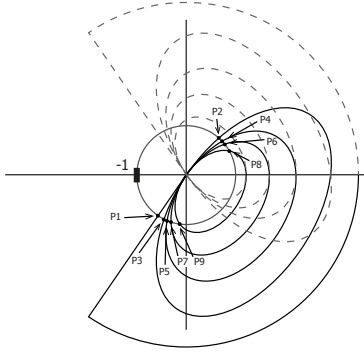


Figure 10: Nyquist of $L(s)$.

6. Verification of the controllers' performance

In this section, numerical simulations and experimental results are shown in order to prove the effectiveness and the advantages of the proposed control to changes in the payload at the tip. The controllers used here were designed in the previous sections. We should state that these three controllers were designed for the case in which the beam has no payload at the tip, and with the same specifications: *minimize the damping coefficients of the first vibration mode*. In this section, we shall change the payload at the tip and keep the designed controllers in order to study the robustness of the control techniques considered to tip payload variations. We shall also check the spillover insensitivity of these controllers.

6.1. Implementation of the fractional-order controller

We first outline the implementation of the fractional-order controller (25), which is rewritten as:

$$C(s) = -\frac{1392.72}{s^{1.25}} = -\frac{1392.72}{s^2} s^{0.75} \quad (26)$$

The fractional term of expression (26) is implemented using the following expression:

$$y_c(t) = T_s^{-\alpha} \sum_{j=0}^{N-1} (-1)^j \binom{-\alpha}{j} f(t - jT_s); \quad (27)$$

where f is the input to the block $s^{0.75}$, $y_c(t)$ is its output, N is the number of terms involved in this discrete convolution, $\alpha = 0.75$, T_s is the sampling period and the combinatorial has been generalized in the following respect:

$$\binom{\beta}{l} = \frac{\beta(\beta+1)\dots(\beta-l+1)}{l!}. \quad (28)$$

Expression (27) has been obtained using the Grünwald-Letnikov (GL) definition of the discretized fractional operator Vinagre et al. (2000). Moreover, we have applied the short memory approximation described in Podlubny (1998) with $N=500$.

Figure 11 shows a good agreement between the frequency responses of $s^{0.75}$ and its discretized implementation (27) with a sampling period of $T_s=0.001$ s, as regards magnitude and phase (maximum error of 4°) in the range of angular frequencies $\in [2, 250]$, which includes all the vibration modes (see Table 2) and the gain crossover frequencies (see Table 3) of the different cases.

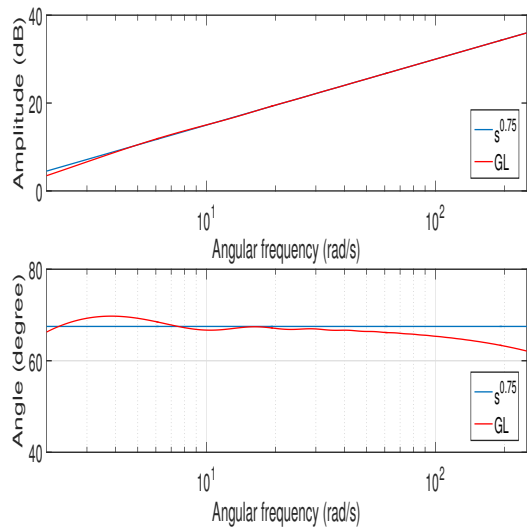


Figure 11: Fractional-order approximation.

	1 st mode			2 nd mode		3 rd mode		4 th mode	
Mass	P1	P2	P3	P4	P5	P6	P7	P8	P9
Mass	-112.20°	66.61°	-112.30°	64.13°	-110.30°	53.34°	-100.80°	34.81°	-85.45°
Mass	-112.00°	66.41°	-112.41°	64.95°	-111.05°	43.31°	-93.22°	32.82°	-82.28°
Mass	-111.80°	66.15°	-112.46°	65.20°	-111.41°	53.28°	-101.53°	29.51°	-81.86°

Table 4: Phase of the Nyquist plot when it crosses the unity circumference

The Pc utilized is a Dell Vostro 410 Desktop Computer with an Intel(R) Core(TM) 2 Quad Q6600 Processor running at 2.4 GHz and equipped with 3GB of DDR2 RAM memory running under Windows XP 32 bits. In order to sample the measurements from the sensors and to produce the analog signals utilized to drive the piezoelectric amplifiers, the PC is equipped with a PCI-6221 data acquisition card from National Instruments. Since the operating system is not designed for real-time applications, the minimum achievable sampling time (even without performing any computation) is 1ms. It is important to note that the computational burden of the different control algorithms did not increase the sampling time, signifying that they are performed in a small fraction of the sampling time.

Since the sampling time achieved on the experimental platform was constant and the combination of the G1-Algorithm and the Short Memory Principle were utilized to compute the Grünwald-Letnikov definition of the discretized fractional operator, the implementation of the fractional operator becomes a convolution of a set of precomputed coefficients stored in a fixed array of numeric values and a set of the last N inputs to the fractional operator stored in a circular array (where N are the number of elements utilized in the approximation of the Short Memory Principle). This signifies that the overall complexity as regards computing this control scheme is constant in each iteration and implies N additions and N multiplications.

The remaining control algorithms have been implemented by approximating their continuous transfer functions using the Runge-Kutta-4 method, which has a constant complexity in each iteration of 39 additions and 39 multiplications for the IRC controller, 38 additions and 38 multiplications for the PPF controller and, in the case of the MPPF controller, 58 additions and 57 multiplications.

6.2. Simulation results

Numerical simulations of the closed-loop control of the flexible beam are carried out. These use MATLAB/SIMULINK and the four different control techniques proposed are compared for the three different

cases: a) without a payload, b) with a payload of 0.15 kg at the tip and c) with a payload of 0.3 kg at the tip. The parameters of the models which are used in the simulations are listed in Table 2. The system is excited using a sinusoidal perturbation applied to the voltage of the piezoelectric actuators. During both simulation and experimentation this signal is therefore defined as:

$$V_p(t) = 3.2 \sin(\omega_1 t) + 0.4 \sin(\omega_2 t) \quad \text{if } t < t_c.$$

Note that this signal is the output of the controller, multiplied or not multiplied by -1 , depending on the technique (see Figures 5 and 6) when $t \geq t_c$. ω_1 and ω_2 are the natural frequencies associated with the first and the second vibration mode of the link. The choice of this perturbation was made with the intention of exciting the two first modes of the link. $V_p(t)$ will therefore be different depending on the mass at the tip of the link (ω_1 and ω_2 change). Moreover, t_c is the commutation time of the excitation and was chosen such that the signal $V_p(t)$ is zero in this instant in order not to have discontinuities in the input signal when the commutation is carried out. We chose to commute $V_p(t)$ after three complete cycles of this signal in order to excite the system during a significant period of time. The control schemes are disabled during the period $0 < t \leq t_c$ because during this period of time the system is been excited in order to produce a similar perturbation for each control scheme. In this section, the results are shown after exciting the system such that the control schemes are enabled from the beginning.

6.2.1. Case a)

Figure 12 shows the voltages measured by the gauges located at the base of the beam. This voltage is proportional to the torque at the base of the beam. This figure plots the responses of the different controllers designed in previous sections and the response when no control is applied (open-loop). It will be observed that the four techniques remove the vibrations of the beam effectively. However, it is important to stress that the fractional-order controller removes the vibration much faster than the other techniques.

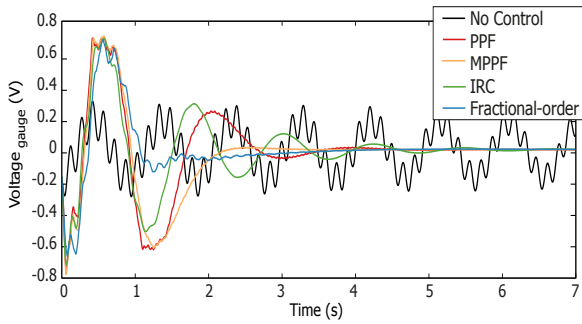


Figure 12: Response in the case of the beam without a payload.

Figure 13 shows the fast fourier transform (FFT) of the previous signals in order to illustrate the damping achieved in the first two modes by the four control techniques. It again shows that the fractional-order controller has the highest efficiency.

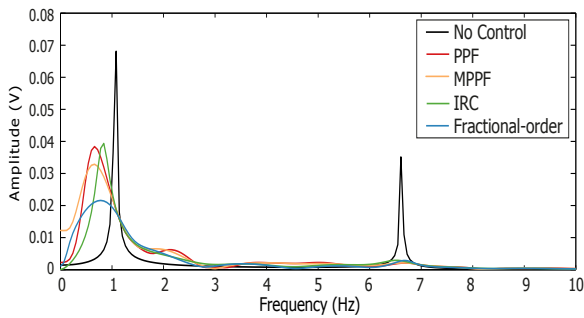


Figure 13: FFT in the case of the beam without a payload.

6.2.2. Case b)

Figure 14 also shows the voltage measured by the gauges for the four different techniques but now using the beam with a payload of 0.15 kg at the tip. The response of the fractional-order controller is now slightly slower than in the case of the beam without a payload at the tip. However, the responses of the other three techniques get considerably worse than in the case without a payload. It is thus possible to state that the fractional-order controller performs much better than the others.

Figure 15 shows the FFT of the signals of the previous figure, again showing the better vibration attenuation provided by the fractional-order controller.

6.2.3. Case c)

Figure 16 also shows the voltage measured by the gauges for the three different techniques but now using

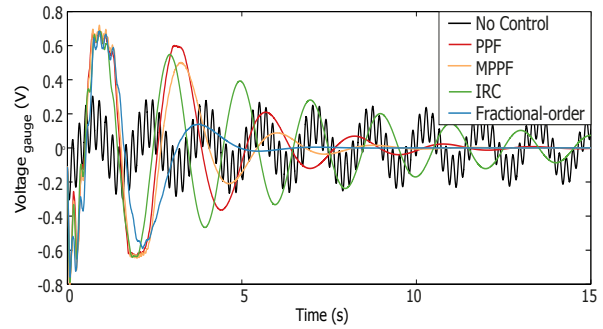


Figure 14: Response in the case of the beam with 0.15 kg.

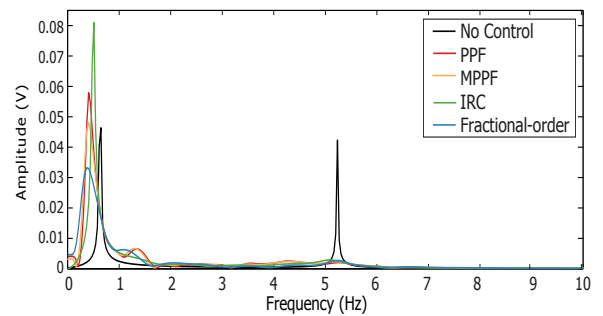


Figure 15: FFT in the case of the beam with 0.15 kg.

the beam with a payload of 0.3 kg at the tip. In this case, the responses of the beam get significantly worse using the three techniques. This is owing to the fact that the mass of the tip payload is excessive, since it is similar to the mass of the beam. However, even in this case, it will be observed that the response using the fractional-order controller is much better than the response produced by the other techniques.

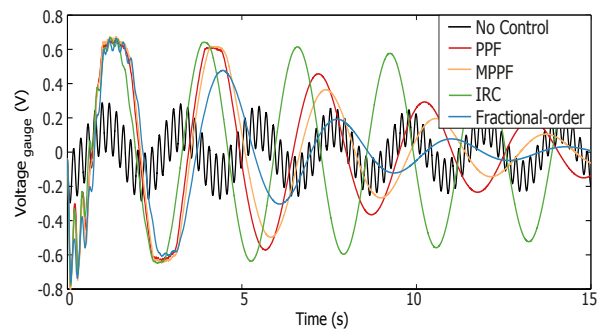


Figure 16: Response in the case of the beam with 0.3 kg.

Figure 17 depicts the FFT of the signals of the above figure, again showing the better attenuation effective-

ness of the fractional-order controller.

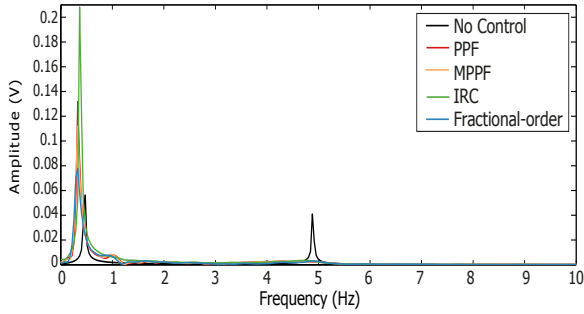


Figure 17: FFT in the case of the beam with 0.3 kg.

6.3. Experimental results

Experiments were carried out with the different controllers. The piezoelectric actuators and the strain gauges placed at the base were used in order to implement the control systems. Moreover, a Polytec LDV laser sensor was used as an external sensor to measure the displacement of the tip of the beam and to assess the effectiveness of the different control schemes in removing the vibrations. The controllers previously designed for the case of zero payload, which were used in the simulations, have also been used here.

6.3.1. Case a)

Figure 18 shows the displacements of the tip of the beam measured by the Polytec LDV in the cases of using the three proposed controllers with the beam without a payload at the tip. It will be observed that the IRC and the fractional-order controllers remove the vibration of the beam effectively. It will also be observed that the fractional-order controller removes the vibration much faster than the IRC controller. However, note that the PPF controller reduces the vibration with regard to the system without control, but a residual vibration remains which is caused by the saturation that this control system produces in the piezoelectric actuator. The saturation voltage of the PEA is $\pm 10V$. Figure 19 shows the voltages of the piezoelectric actuators for the four techniques, illustrating the saturation produced by the PPF.

6.3.2. Case b)

Figure 20 shows the displacement of the tip of the beam in the case of a payload of 0.15 kg at the tip. The responses of the IRC and the fractional-order controllers show that these controllers damp the vibration, but significantly more slowly than in case a). The fractional-order controller again removes the vibrations faster than

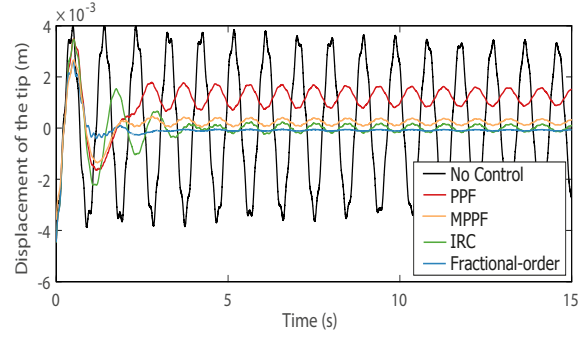


Figure 18: Displacement in the case of the beam without a payload.

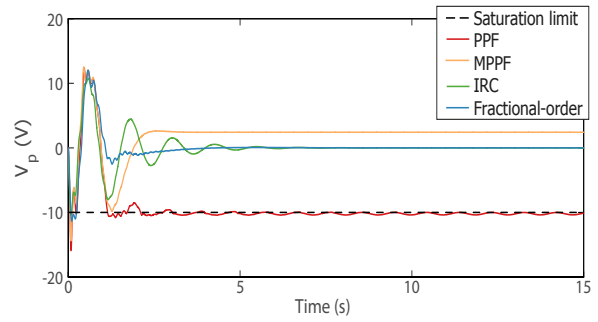


Figure 19: Voltage applied to the piezoelectric actuators.

the IRC controller. The PPF controller produces a very small damping of the vibration because it again saturates the PEA.

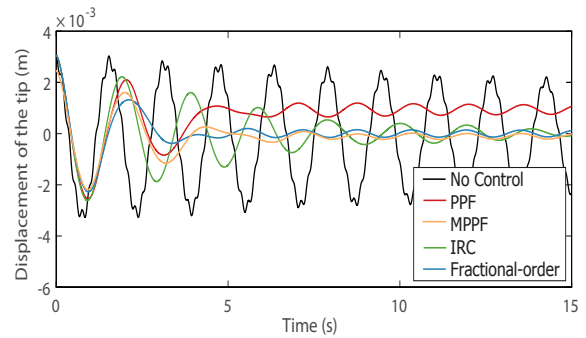


Figure 20: Displacement in the case of the beam with 0.15 kg.

6.3.3. Case c)

Figure 21 shows the displacement of the tip of the beam in the case of a payload of 0.3 kg at the tip. The responses of the IRC and the fractional-order controllers show that these controllers damp the vibrations, but more slowly than in case b). The fractional-order

controller again removes the vibrations faster than the IRC controller.

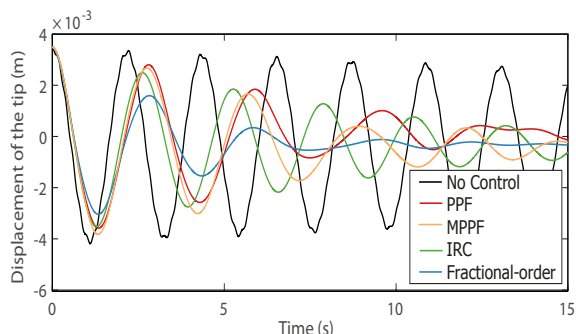


Figure 21: Displacement in the case of the beam with 0.3 kg.

6.4. Discussion

The results obtained in the two previous subsections are compared and discussed as follows.

1. The phase margins of the PPF and MPPF are very small. The phase margin of the IRC is acceptable for the nominal case (no payload), although it becomes quite small when the payload is 0.3 kg. The phase margin of the FI is very good for all the payloads.
2. The phase margin of the IRC diminishes significantly as the payload increases. However, the phase margin of the FI is very robust, remaining approximately constant with all the payloads.
3. The phase margin of the FI always remains lower than $-90\alpha = -112.5^\circ$, as was stated in the design procedure of the FI.
4. The gain margin M_g is infinite in both the IRC and the FI controllers, as a consequence of adding D_f to $G_i(s)$ and multiplying the result by -1 . However, the gain margin is very low in the PPF and MPPF (it is very close to 1).
5. The gain crossover frequency ω_c diminishes in all the controllers as the payload increases, i.e., the closed-loop system becomes slower. This reduction is similar in the IRC and the FI: the ratio between the ω_c with the maximum payload and the ω_c with no payload is about 0.45 in both controllers. However, ω_c undergoes smaller variations with payload changes in the case of the PPF controller.

Table 5 shows the damping achieved by the proposed controllers in the first two vibration modes. These results were obtained by calculating the damping of the poles of the closed-loop associated with the two first vibration modes. It will be observed that the controller that attains the most damping is the FI, the second is the PPF, the third the MPPF, and that which provides the least damping is the IRC.

Table 6 shows the specifications of the responses obtained in the experiments. This table lists the settling time t_s - defined as the time that the response needs to enter the band of ± 1 mm -, the damping ξ and the maximum amplitude of the response AV_1 . This table shows that:

1. The settling time t_s of the responses increases as the gain crossover frequency ω_c diminishes.
2. The FI controller damps the vibrations much faster than the IRC controller. In fact, the settling time achieved with the FI is significantly smaller than that achieved with the MPPF and IRC in all the payload cases. The PPF is unable to reduce the vibrations to an amplitude of 1 mm.
3. The experiments show that the FI controller attains a damping ξ_1 of approximately twice the damping attained with the IRC. Note that the second vibration mode is very small in all the experiments, and it was not therefore possible to estimate the damping ξ_2 of this mode.
4. The experiments show that there are no spillover effects in the IRC and FI control systems, in accordance with the properties that are theoretically achieved with these controllers.

Finally, we should mention that since we wished to illustrate that our control system is robust to spillover, we have chosen quite a large beam such that several vibration modes could be clearly noticed. For this reason, our beam is larger than others shown in scientific literature. Moreover, we use a single piezoelectric patch, while other prototypes may include several patches, which implies that we can apply less torque to our beam than others. These facts make the dynamics of our beam slower than others and, consequently, the closed-loop dynamics expected using our controller should also be slower. For example:

1. Our beam is 1 m long, 4 vibration modes can be noticed, and the settling time for the nominal payload (0 Kg) obtained using our fractional-order controller is about 1 s.

	<i>IRC</i> (0kg)	<i>IRC</i> (0.15kg)	<i>IRC</i> (0.3kg)	<i>PPF</i> (0kg)	<i>PPF</i> (0.15kg)	<i>PPF</i> (0.3kg)	<i>MPPF</i> (0kg)	<i>MPPF</i> (0.15kg)	<i>MPPF</i> (0.3kg)	<i>FI</i> (0kg)	<i>FI</i> (0.15kg)	<i>FI</i> (0.3kg)
ξ_1	0.166	0.0533	0.0104	0.43	0.1737	0.0707	0.284	0.125	0.0578	0.67	0.35	0.12
ξ_2	0.053	0.0651	0.0622	0.724	0.72	0.626	0.869	0.827	0.69	0.347	0.62	0.75

Table 5: Dampings

	<i>IRC</i> (0kg)	<i>IRC</i> (0.15kg)	<i>IRC</i> (0.3kg)	<i>PPF</i> (0kg)	<i>PPF</i> (0.15kg)	<i>PPF</i> (0.3kg)	<i>MPPF</i> (0kg)	<i>MPPF</i> (0.15kg)	<i>MPPF</i> (0.3kg)	<i>FI</i> (0kg)	<i>FI</i> (0.15kg)	<i>FI</i> (0.3kg)
$t_s(s)$	1.8	5.0	8.1	—	—	9.5	1.4	3.5	7.8	0.7	2.3	4.9
ξ_1	0.06	0.022	0.008	0.19	0.064	0.027	0.12	0.075	0.026	0.28	0.15	0.04
AV_1mm	2.2	2.1	2.7	3.5	2.0	2.9	2.5	1.8	2.8	2.5	2.1	3.0

Table 6: Experimentation

2. The beam used in Banks et al. (2002) is 0.286 m long, 3 vibration modes are considered, and the closed-loop settling time is about 1 s.
3. The beam used in Aphale et al. (2007) is 0.5 m long, 3 vibration modes are considered, and the closed-loop settling time is about 1 s.
4. The beam used in Meurer et al. (2008) is 0.047 m long, 1 vibration mode is visible, and the closed-loop settling time is about 20 ms. The settling time of this control system is much lower than the others but this beam is also much shorter.

However, the settling time achieved using our controller is similar to those achieved in these examples, which propose controllers that are applied to significantly shorter beams, with much less rotational inertia to be turned. This justifies that our controller is more efficient than others. The settling time becomes longer when a payload is added at the tip. Since no data is provided in other works about how the dynamics of their proposed control systems are slowed by an increase in the tip payload, the effects of tip payload changes have been compared when all of these controllers have been applied to the same beam (our experimental setup). Table 5 shows that our controller damps the vibrations faster than the other controllers.

7. Conclusions

This paper has addressed the control of vibrations in collocated smart structures. We have shown that a very simple fractional-order controller - a FI controller - significantly improves the performance and robustness of three well-known integer-order control schemes used in smart structures, the IRC, PPF and MPPF controllers.

Improvement to the closed-loop response is achieved by exploiting the property of CPE elements (FI controllers in this paper) of adding/subtracting a constant phase to the frequency response of the plant at all frequencies ($0 \leq \omega < \infty$). Using an FI therefore allows the Nyquist plot to be conveniently approximately rotated in such a way that the phase margin of the open-loop transfer function is augmented. Moreover, we have demonstrated that, by doing this in collocated smart structures, the robustness of the system can be significantly augmented in several ways: a) the phase margin is maintained approximately constant to changes in the payload at the tip of the beam (which implies increased stability robustness and damping robustness), b) this phase margin (or damping) is also guaranteed for all the vibration modes, with which spillover effects are prevented and c) the gain margin is always infinite for any tip payload, thus achieving a very high robustness to plant gain changes.

We should state that, in order to achieve these frequency response features, some manipulations are needed which are similar to those carried out in the IRC control scheme: a negative gain must be connected in parallel to the plant and a sign inversion is subsequently carried out. By doing this, robustness to spillover effects and an infinity gain margin is achieved in both the IRC and the FI. However, the FI guarantees a minimum phase margin for any change in the tip payload, in contrast to the IRC.

With regard to the other control schemes, the PPF and MPPF can effectively damp the first vibration mode. However, if there are any uncertainties in the plant parameters, or they are time-varying owing to, for example, the presence of a tip mass, the effectiveness of these two controllers deteriorates. The PPF and MPPF controllers are insensitive to spillover because, since they

include a second-order low-pass filter, their frequency responses roll off quickly at high frequencies. However, if there is a bias term in the measurement of the sensor, the control action can saturate, as was shown in the experimental results.

In summary, IRC, PPF, MPPF and FI controllers share the properties (which are not fulfilled simultaneously by other controllers in scientific literature) of being robust to spillover and robustly stable to large changes in most of the parameters of the plant. Moreover, the IRC and FI controllers share the property (which is not fulfilled by the PPF and the MPPF) of having an infinite gain margin, which implies stability robustness to very large gain changes. Finally, the FI has the advantage over the IRC, and also over the PPF and the MPPF, of being robust in its phase margin (the absolute value of the phase margin is always greater than a chosen value, which is defined by the fractional order of the controller) when the system undergoes large changes in its parameters. This last feature guarantees a minimum relative stability and a minimum damping of the smart structure in the case of large parametric variations. We should state that this robust property is not achieved by any other control method.

Simulated and experimental results have demonstrated the superior performance and robustness of the FI controller over the IRC, the PPF and the MPPF as regards controlling collocated smart structures. However, a discrepancy in the damping can be observed between simulated and experimental results in all the four controllers. Some preliminary tests show that this may be caused by the non-negligible offset of the strain sensor (although we attempted to minimize this prior to each experiment) and the nonlinear effects of the hysteresis of the piezoelectric actuator. Finding means to reduce these effects on the fractional-order control will be the object of our future research.

8. Acknowledgments

This research was sponsored in part by the Spanish FPU12/00984 and FPU14/02256 Program (Ministerio de Educacion, Cultura y Deporte), in part by the Spanish Government Research Program with the project DPI2012-37062-CO2-01 (Ministerio de Economía y Competitividad) and in part by the European Social Fund.

References

Aphale, S. S., Fleming, A. J., & Moheimani, S. O. R. (2007). Integral resonant control of collocated smart structures. *Smart Materials and Structures*, 16(2), 439–446.

- Banks, H., del Rosario, R., & Tran, H. (2002). Proper orthogonal decomposition-based control of transverse beam vibrations: experimental implementation. *IEEE Trans. Control Systems Technology*, 10(5), 717–726.
- Banks, H., Smith, R., & Wang, Y. (1996). *Smart Material Structures: Modeling, Estimation and Control*. Masson/John Wiley, Paris/Chichester.
- Bar-Kana, I., Fischl, R., & Kalata, P. (1991). Direct position plus velocity feedback control of large flexible space structures. *IEEE Trans. Automatic Control*, 36(10), 1186–1188.
- Bohannan, G. W. (2008). Analog fractional order controller in temperature and motor control applications. *Journal of Vibration and Control*, 14(9-10), 1487–1498.
- Chu, Z. & Cui, J. (2015). Experiment on vibration control of a two-link flexible manipulator using an input shaper and adaptive positive position feedback. *Advances in Mechanical Engineering*, 7(10).
- Cole, K. S. (1933). Electric conductance of biological systems. In *Cold Spring Harbor symposia on quantitative biology*, volume 1 (pp. 107–116).: Cold Spring Harbor Laboratory Press.
- Fanson, J. & Caughey, T. (1990). Positive position feedback-control for large space structures. *AIAA J.*, 28(4), 717–724.
- Feliu, V. & Feliu, S. (1997). A method of obtaining the time domain response of an equivalent circuit model. *Journal of Electroanalytical Chemistry*, 435(1-2), 1–10.
- Fleming, A., Aphale, S., & Moheimani, S. R. (2010). A new method for robust damping and tracking control of scanning probe microscope positioning stages. *IEEE Trans. Nanotechnology*, 9(4), 438–448.
- Friswell, M. I. & Inman, D. J. (1999). The relationship between positive position feedback and output feedback controllers. *Smart Materials and Structures*, 8(3), 285–291.
- Ghosh, S., Sahu, A., & Bhattacharya, P. (2015). Observer-based h_2 -robust controller for active vibration control of laminated composite plates with an optimally placed ide-pfc actuator. *J. Aerospace Eng.*
- Goh, C. J. & Caughey, T. K. (1985). On the stability problem caused by finite actuator dynamics in the collocated control of large space structures. *International Journal of Control*, 41(3), 787–802.
- Halim, D. & Moheimani, S. (2002a). Experimental implementation of spatial h_∞ control on a piezoelectric laminate beam. *IEEE/ASME Trans. Mechatronics*, 7(3), 346–356.
- Halim, D. & Moheimani, S. (2002b). Spatial h_2 control of a piezoelectric laminate beam: experimental implementation. *IEEE Trans. Control Systems Technology*, 10(4), 533–546.
- Manabe, S. (2002). A suggestion of fractional-order controller for flexible spacecraft attitude control. *Nonlinear Dynamics*, 29(1/4), 251–268.
- McEver, M. & Leo, D. J. (2001). Autonomous vibration suppression using on-line pole-zero identification. *ASME Journal of Vibration and Acoustics*, 123(3), 487–495.
- Meurer, T., Thull, D., & Kugi, A. (2008). Flatness-based tracking control of a piezoactuated eulerbernoulli beam with non-collocated output feedback: theory and experiments. *International Journal of Control*, 81(3), 475–493.
- Moheimani, S. R. & Fleming, A. J. (2005). *Piezoelectric Transducers for Vibration Control and Damping*. London: Springer.
- Monje, C., Ramos, F., Feliu, V., & Vinagre, B. (2007). Tip position control of a lightweight flexible manipulator using a fractional order controller. *Control Theory & Applications, IET*, 1(5), 1451–1460.
- Monje, C. A., Calderon, A. J., Vinagre, B. M., Chen, Y., & Feliu, V. (2004). On fractional PI^λ controllers: some tuning rules for robustness to plant uncertainties. *Nonlinear Dynamics*, 38(1-4), 369–381.

- Monje, C. A., Vinagre, B. M., Feliu, V., & Chen, Y. (2008). Tuning and auto-tuning of fractional order controllers for industry applications. *Control Engineering Practice*, 16(7), 798–812.
- Nima Mahmoodi, S. & Ahmadian, M. (2009). Active vibration control with modified positive position feedback. *ASME Journal of Dynamic Systems, Measurement, and Control*, 131(4), 8.
- Nima Mahmoodi, S., Ahmadian, M., & Inman, D. J. (2010). Adaptive modified positive position feedback for active vibration control of structures. *Journal of Intelligent Material Systems and Structures*, 21(6), 571–580.
- Omid, E., Mahmoodi, S. N., & Shepard, W. S. (2015). Vibration reduction in aerospace structures via an optimized modified positive velocity feedback control. *Aerospace Science and Technology*, 45, 408–415.
- Padula, F. & Visioli, A. (2012). Optimal tuning rules for proportional-integral-derivative and fractional-order proportional-integral-derivative controllers for integral and unstable processes. *Control Theory & Applications, IET*, 6(6), 776–786.
- Petersen, I. & Pota, H. (2003). Minimax l_q optimal control of a flexible beam. *Control Engineering Practice*, 11(11), 1273–1287.
- Piersol, A. & Bendat, J. (1993). *Engineering applications of correlation and spectral analysis*. New York: Wiley Interscience.
- Podlubny, I. (1998). *Fractional differential equations: an introduction to fractional derivatives, fractional differential equations, to methods of their solution and some of their applications*, volume 198. Academic press.
- Pota, H. & Alberts, T. (1995). Multivariable transfer functions for a slewing piezoelectric laminate beam. *ASME Journal of Dynamic Systems, Measurement, and Control*, 117(3), 352–359.
- Pota, H. R., Moheimani, S. O. R., & Smith, M. (2002). Resonant controllers for smart structures. *Smart Materials and Structures*, 11(1), 1–8.
- Preumont, A. (2011). *Vibration Control of Active Structures: An Introduction*. Springer Science & Business Media, Springer.
- Preumont, A., Bastait, R., & Rodrigues, G. (2009). Scale effects in active optics of large segmented mirrors. *Mechatronics*, 19(8), 1286–1293.
- Quintana, A. & Ciurana, J. (2011). Chatter in machining processes: a review. *International Journal of Machine Tools & Manufacture*, 51, 363–376.
- Tavazoei, M. S. & Tavakoli-Kakhki, M. (2014). Compensation by fractional-order phase-lead/lag compensators. *IET Control Theory & Applications*, 8(5), 319–329.
- Tokhi, O. & Veres, S. (2002). *Active Sound and Vibration Control*. IEE Control Engineering Series 62, Institution of Electrical Engineers.
- Valerio, D. (2005). Fractional robust system control. *Instituto Superior Técnico, Universidade Técnica de Lisboa*.
- Vepa, R. (2010). *Dynamics of Smart Structures*. John Wiley & Sons, Ltd.
- Vinagre, B., Podlubny, I., Hernandez, A., & Feliu, V. (2000). Some approximations of fractional order operators used in control theory and applications. *Fractional Calculus and Applied Analysis*, 3(3), 231–248.
- Zhu, X., Liu, J., Huang, Q., & Gao, S. (2009). Robust h_∞ control in active vibration control of piezoelectric smart structure. In *Proceedings 9th International Conference on Electrical Measurement and Instruments, ICEMI'2009* (pp. 694–698).: IEEE.